INTERNATIONAL JOURNAL OF HYDROGEN ENERGY XXX (2012) 1–6

Available online at www.sciencedirect.com

SciVerse ScienceDirect

journal homepage: www.elsevier.com/locate/he

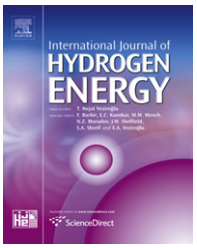

Non-linear aeroelastic behavior of large horizontal-axis wind turbines: A multibody system approach

C.G. Gebhardt [a,c,*], S. Preidikman [a,c], M.H. Jørgensen [b], J.C. Massa [a]

[a] Department of Structures, National University of Cordoba, 1611 Vélez Sarsfield Avenue, 5016 Córdoba, Argentina
[b] Department of Mechanical and Manufacturing Engineering, Aalborg University, 16 Fibigerstræde, 9220 Aalborg East, Denmark
[c] CONICET, 1917 Rivadavia Avenue, 1033 Buenos Aires, Argentina

ARTICLE INFO

Article history:
Received 28 October 2011
Accepted 12 December 2011
Available online xxx

Keywords:
Wind turbines
Rigid-flexible multibody systems
Aerodynamics
Aeroelasticity

ABSTRACT

In this paper, we present the development of a rigid-flexible multibody model which, coupled with an existing aerodynamic model, is used to numerically simulate the non-linear aeroelastic behavior of large horizontal-axis wind turbines. The model is rather general, different configurations could be easily simulated though it is primarily intended to be used as a research tool to investigate influences of different dynamic aspects. It includes: *i*) a supporting tower; *ii*) a nacelle which contains the electricity generator, the power electronics and the control systems; *iii*) a hub, where the blades are fixed, connected to the generator rotating shaft; and, *iv*) three blades which extract energy from the airstream.

The blades are considered flexible, and their equations of motion are discretized in space domain by using beam finite elements capable of taking into account the non-linearities coming from the kinematics. The tower is also considered flexible, but its equations of motion are discretized by using the method of assumed-modes. The nacelle and hub are considered rigid, and their equations of motion take into account the effects of the kinematic non-linearities.

Due to the system complexity, the tower, nacelle and hub are modeled as a single kinematic chain and each blade is modeled separately. Constraint equations are used to connect the blades to the hub. The resulting governing equations are differential-algebraic, and these are numerically and interactively solved in the time domain by using a fourth order predictor-corrector scheme.

The results help to understand the wind speed influence on: *i*) the rotor angular speed; *ii*) the after-forward and side-to-side displacements of the tower; and, *iii*) the flap- and edge-wise displacements of the blades.

1. Introduction

During the last two decades, due to the necessity to obtain clean sources of energy, the interest in designing wind turbines increasingly large has been growing steadily. To obtain efficient designs, it is necessary to develop precise and robust techniques capable to predict the aeroelastic characteristics of such systems. Across the years pursuing this

* *Corresponding author*. Department of Structures, National University of Cordoba, 1611 Vélez Sarsfield Avenue, 5016 Córdoba, Argentina.
E-mail addresses: cggebhardt@yahoo.com.ar, cgebhardt@efn.uncor.edu (C.G. Gebhardt).

0360-3199/$ – see front matter Copyright © 2011, Hydrogen Energy Publications, LLC. Published by Elsevier Ltd. All rights reserved.
doi:10.1016/j.ijhydene.2011.12.090

target, several authors have been developing structural models to study the dynamic behavior of Large Horizontal-Axis Wind Turbines (LHAWTs) and very different approaches have been explored.

Petersen [1] presented a time domain model for simulating the dynamic response of a horizontal-axis wind turbine. A general kinematic analysis was used to derive the local inertial loads. The wind turbine is subdivided into three substructures: the tower, the nacelle-shaft and the rotor-blades. The model is discretized using the finite element technique. Lee et al. [2] developed a methodology representing the wind turbine as a multi-flexible-body system with both, rigid and flexible body sub-systems. Rigid body sub-systems (nacelle and hub) are modeled using Kane's equations, and flexible body sub-systems (tower and blades), using geometrically exact, non-linear beam finite elements. Jonkman and Buhl [3] developed FAST code which is a comprehensive aeroelastic simulator. FAST model employs a combined modal and multibody dynamics formulation. Blades and tower are characterized using a linear modal representation while the remaining components are modeled as rigid bodies. Zhao et al. [4] developed a methodology based on hybrid multibody systems composed of rigid, flexible bodies, force elements and joints. Using a cardanic joint beam element, the flexible bodies are modeled as sets of rigid bodies connected by cardanic joints; thus a whole wind turbine structure can be represented by a discrete system of rigid bodies, springs, and dampers. A very detailed study focused on the rotor blade was developed by Kallesøe [5], who proposed an extension of Hodges-Dowell's Partial Differential Equations (PDEs) of blade motion [6] by including the effects of gravity, pitch action and rotor speed variations. The PDEs of motion are approximated by Ordinary Differential Equations (ODEs) of motion using an assumed-modes method.

In this paper, we present a reduced order structural model of a three-bladed LHAWT. The blades are considered flexible, and their Equations of Motion (EoMs) are discretized in space domain by using beam finite elements capable of taking into account the non-linearities coming from the kinematics. The tower is also considered flexible, but its EoMs are discretized using the method of assumed-modes. The nacelle and hub are considered rigid, and are represented by a geometric formulation which allows taking into account the effects of the kinematic non-linearities [7,8]. The presented model involves different modeling approaches; in addition, the combination of different techniques for modeling the LHAWT components renders a very precise reduced order model. For solving the LHAWT-EoMs in the time domain, a scheme based on a modified version of the fourth order Hamming's predictor-corrector method is used [9].

2. Dynamic model

2.1. Tower, nacelle and hub

In this work, the tower, nacelle and hub are considered members of a single kinematic chain. It means that the position and orientation of any given point belonging to the nacelle is related to the tower, whereas the position and orientation of any given point belonging to the hub is related to the nacelle.

The tower is modeled as a straight prismatic, linearly elastic, undamped beam. The root of the tower is rigidly attached to the ground and the nacelle is mounted at its top. The assumed-modes method [10,11] is used to obtain a tower model with few Degrees of Freedom (DoFs). We consider a mode for the after-forward bending, a mode for the side-to-side bending and another one for torsion about the longitudinal axis.

The nacelle and hub are modeled as rigid bodies. The nacelle can rotate respect to the tower in a yaw angle, which is commanded by the control system. The hub can freely rotate respect to the nacelle in an azimuth angle. Both rotations are represented by a sequence of Euler's angles.

The EoMs for the tower, nacelle and hub as a single kinematic chain can be expressed in the form

$$[\mathbf{M}_{tnh}]\{\ddot{\mathbf{q}}_{tnh}\} + [\mathbf{K}_{tnh}]\{\mathbf{q}_{tnh}\} = \{\mathbf{F}^{g}_{tnh} + \mathbf{F}^{k}_{tnh} + \mathbf{F}^{c}_{tnh}\}, \quad (1)$$

where $\mathbf{q}_{tnh}$ is the vector of generalized coordinates, $\mathbf{M}_{tnh}$ and $\mathbf{K}_{tnh}$ are the mass and stiffness matrices, respectively. $\mathbf{F}^{g}_{tnh}$ is the vector of generalized forces accounting the contributions coming from the gravitational field, the control systems and the electricity generator. $\mathbf{F}^{k}_{tnh}$ is a vector of kinematic forces accounting for the centrifugal and Coriolis' effects on the nacelle and hub and $\mathbf{F}^{c}_{tnh}$ is the constraint forces vector due to effects of the blades, which is computed as

$$\mathbf{F}^{c}_{tnh} = -\sum_{i=1}^{3}\left[\frac{\partial \boldsymbol{\varphi}_i}{\partial \mathbf{q}_{tnh}}\right]^{T}\{\boldsymbol{\lambda}_i\}, \quad (2)$$

where $\boldsymbol{\varphi}_i$ is the set of constraint equations corresponding to the i-th blade and $\boldsymbol{\lambda}_i$ is its vector of Lagrange's multipliers [12,13].

At this level, it is important to remark that the aerodynamic loads do not appear explicitly, since these forces directly act over the blades, and their actions on the kinematic chain are implicitly transferred by mean of the Lagrange's multipliers.

2.2. Blades

Each blade is modeled as a non-straight, linearly elastic, undamped beam. We consider, separately, large displacements and rotations due to the motion of the blade as a rigid body, and small displacements and small rotations due to the elastic deformation. The motion of the blade as a whole is called *primary motion* and its elastic motion is called *secondary motion*.

The *primary motion* gives us the position and orientation of the blades. The position is described by using three generalized coordinates and the orientation, by a unit quaternion [8,12], i.e. four constrained generalized coordinates since the addition of their squares must be always equal to one.

The *secondary motion* leads us to a set of PDEs for a continuous elastic medium. To obtain a finite set of ODEs, the blades are discretized using two-noded beam finite elements along the elastic axis, with six DoFs per node. In this work, the structural mesh of each blade has twenty-two nodes.

Please cite this article in press as: Gebhardt CG, et al., Non-linear aeroelastic behavior of large horizontal-axis wind turbines: A multibody system approach, International Journal of Hydrogen Energy (2012), doi:10.1016/j.ijhydene.2011.12.090

The EoMs for *primary motion* of the blade number one can be expressed as

$$\left[\mathbf{M}_1\right]\{\ddot{\mathbf{q}}_1\}+\left[\mathfrak{M}_1\right]\{\ddot{\mathbf{p}}_1\}=\left\{\mathbf{F}_1^g+\mathbf{F}_1^k+\mathbf{F}_1^c\right\}, \tag{3}$$

where $\mathbf{q}_1$ and $\mathbf{p}_1$ are the generalized coordinates for *primary* and *secondary motions*, respectively. $\mathbf{M}_1$ is the mass matrix for *primary motion* and $\mathfrak{M}_1$ is the mass matrix which couples *primary* and *secondary motions*. $\mathbf{F}_1^g$ and $\mathbf{F}_1^k$ are vectors accounting for the generalized and kinematic forces, respectively, and $\mathbf{F}_1^c$ is the constraint forces vector due to the blade-hub attachment, which is computed by

$$\mathbf{F}_1^c=-\left[\frac{\partial\boldsymbol{\varphi}_1}{\partial\mathbf{q}_1}\right]^T\{\boldsymbol{\lambda}_1\}. \tag{4}$$

The EoMs for *secondary motion* of the blade number one can be expressed as

$$\left[\mathbf{m}_1\right]\{\ddot{\mathbf{p}}_1\}+\left[\mathfrak{M}\right]^T\{\ddot{\mathbf{q}}_1\}+\left[\mathbf{k}_1\right]\{\mathbf{p}_1\}=\left\{\mathbf{f}_1^g+\mathbf{f}_1^k\right\}, \tag{5}$$

where $\mathbf{m}_1$ and $\mathbf{k}_1$ are the mass and stiffness matrices, and $\mathbf{f}_1^g$ and $\mathbf{f}_1^k$ are vectors accounting for the generalized and kinematic forces, respectively. These EoMs are reduced in size at every time step by using a modal projection scheme. The EoMs of the blades number two and three are obtained using the same procedure.

2.3. Constraints

The roots of the blades are attached to the hub. Each blade can rotate respect to the hub in a pitch angle, which is commanded by the control system. Six constraint equations establish the linkage between the hub and each blade, three of them to specify position and the other three to specify orientation. An extra constraint equation is required to specify the unit quaternion condition.

The set of algebraic constraint equations for the blade number one can be expressed as [12,13]

$$\boldsymbol{\varphi}_1(\mathbf{q}_{tnh},\mathbf{q}_1)=\mathbf{0}, \tag{6}$$

where only holonomic constraints are considered.

Constraint equations for the blades number two and three are obtained following the same procedure.

2.4. Governing equations

The governing equations for the whole system are Differential-Algebraic Equations (DAEs), since ODEs and algebraic constraint equations are involved. After deriving the constraint equations twice respect to the time, the governing equations can be expressed as

$$\begin{bmatrix}\mathbf{M} & \mathbf{B}^T\\ \mathbf{B} & \mathbf{0}\end{bmatrix}\begin{Bmatrix}\ddot{\mathbf{x}}\\ \boldsymbol{\lambda}\end{Bmatrix}=\begin{Bmatrix}\mathbf{F}\\ -\dot{\mathbf{B}}\dot{\mathbf{x}}\end{Bmatrix}, \tag{7}$$

where

$$\left[\mathbf{M}\right]=\begin{bmatrix}\mathbf{M}_{tnh} & \mathbf{0} & \mathbf{0} & \mathbf{0} & \mathbf{0} & \mathbf{0} & \mathbf{0}\\ \mathbf{0} & \mathbf{M}_1 & \mathfrak{M}_1 & \mathbf{0} & \mathbf{0} & \mathbf{0} & \mathbf{0}\\ \mathbf{0} & \mathfrak{M}_1^T & \mathbf{m}_1 & \mathbf{0} & \mathbf{0} & \mathbf{0} & \mathbf{0}\\ \mathbf{0} & \mathbf{0} & \mathbf{0} & \mathbf{M}_2 & \mathfrak{M}_2 & \mathbf{0} & \mathbf{0}\\ \mathbf{0} & \mathbf{0} & \mathbf{0} & \mathfrak{M}_2^T & \mathbf{m}_2 & \mathbf{0} & \mathbf{0}\\ \mathbf{0} & \mathbf{0} & \mathbf{0} & \mathbf{0} & \mathbf{0} & \mathbf{M}_3 & \mathfrak{M}_3\\ \mathbf{0} & \mathbf{0} & \mathbf{0} & \mathbf{0} & \mathbf{0} & \mathfrak{M}_3^T & \mathbf{m}_3\end{bmatrix} \tag{8}$$

is the system (or global) mass matrix,

$$[\mathbf{B}]=\begin{bmatrix}\frac{\partial\boldsymbol{\varphi}_1}{\partial\mathbf{q}_{tnh}} & \frac{\partial\boldsymbol{\varphi}_1}{\partial\mathbf{q}_1} & \mathbf{0} & \mathbf{0} & \mathbf{0} & \mathbf{0} & \mathbf{0}\\ \frac{\partial\boldsymbol{\varphi}_2}{\partial\mathbf{q}_{tnh}} & \mathbf{0} & \mathbf{0} & \frac{\partial\boldsymbol{\varphi}_2}{\partial\mathbf{q}_2} & \mathbf{0} & \mathbf{0} & \mathbf{0}\\ \frac{\partial\boldsymbol{\varphi}_3}{\partial\mathbf{q}_{tnh}} & \mathbf{0} & \mathbf{0} & \mathbf{0} & \mathbf{0} & \frac{\partial\boldsymbol{\varphi}_3}{\partial\mathbf{q}_3} & \mathbf{0}\end{bmatrix} \tag{9}$$

is the system (or global) constraint jacobian matrix,

$$\mathbf{x}=\{\,\mathbf{q}_{tnh}\quad\mathbf{q}_1\quad\mathbf{p}_1\quad\mathbf{q}_2\quad\mathbf{p}_2\quad\mathbf{q}_3\quad\mathbf{p}_3\,\}^T \tag{10}$$

is the generalized coordinates vector, and

$$\boldsymbol{\lambda}=\{\,\lambda_1\quad\lambda_2\quad\lambda_3\,\}^T \tag{11}$$

is the Lagrange's multipliers vector, and

$$\mathbf{F}_{tnh}=\begin{Bmatrix}-\mathbf{K}_{tnh}\mathbf{q}_{tnh}+\mathbf{F}_{tnh}^g+\mathbf{F}_{tnh}^k\\ \mathbf{F}_1^g+\mathbf{F}_1^k\\ -\mathbf{k}_1\mathbf{p}_1+\mathbf{f}_1^g+\mathbf{f}_1^k\\ \mathbf{F}_2^g+\mathbf{F}_2^k\\ -\mathbf{k}_2\mathbf{p}_2+\mathbf{f}_2^g+\mathbf{f}_2^k\\ \mathbf{F}_3^g+\mathbf{F}_3^k\\ -\mathbf{k}_3\mathbf{p}_3+\mathbf{f}_3^g+\mathbf{f}_3^k\end{Bmatrix} \tag{12}$$

is the forces vector which contains all the contributions explained in previous subsections.

3. Aerodynamic loads

Let us consider a body immersed in a fluid stream. When the Reynolds' number is large, the viscous effects can be confined to those regions close to the solid surface; these vorticity-dominated regions are called boundary layers. Part of the vorticity contained in the boundary layers is shed downstream into the flow field, where it can only be transported by the fluid particles, but neither created nor destroyed. This transported vorticity forms the wakes behind the body.

The thickness of the boundary layers and wakes tends to zero when the Reynolds' number tends to infinity. Under this condition, the boundary layers and wakes can be represented as continuous bounded and free sheets of vorticity, respectively.

In the Unsteady Vortex-Lattice Method (UVLM), the continuous bounded vortex sheets of the boundary layers are discretized into a lattice of short, straight vortex segments of constant circulation. These segments divide the surface of the

Please cite this article in press as: Gebhardt CG, et al., Non-linear aeroelastic behavior of large horizontal-axis wind turbines: A multibody system approach, International Journal of Hydrogen Energy (2012), doi:10.1016/j.ijhydene.2011.12.090

body into a finite number of area elements. The model is completed by joining free vortex lines, representing the continuous free vortex sheets of the wakes, to the bounded vortex lattice along the separation sharp edges where the separation takes place. In our study case, the separation edges are the trailing edges and tips of the blades.

Each area element in the lattice is enclosed by a loop of vortex segments. To reduce the size of the problem, each element is considered to be enclosed by a closed loop of vortex segments having the same circulation, i.e. vortex rings of constant circulation. Then the spatial conservation of circulation is automatically satisfied.

The circulation of the vortex rings are determined by using a discrete version of the non-penetration boundary condition; the fluid cannot penetrate the solid surface, taking into account the contribution of the free stream, the wakes and the velocity of the solid surface. At each time step, after determining the rings circulations, vortex segments are shed into the flow field and become part of the grids that approximate the free vortex sheets of the wakes.

By using an extended version of the UVLM developed by Gebhardt et al. [14], we estimate the magnitude and evolution of the aerodynamic loads in the time domain. This version allows considering the presence of both, the tower and the land-surface boundary layer. The capability to capture these phenomena is a novel aspect of our aerodynamic model.

4. Numerical integration scheme

The second-order governing differential equations have to be re-written as a first order system and integrated in time domain as follows:

1. At $t = 0$ the initial conditions are known.
2. At $t = \Delta t$ the solution is predicted by the explicit Euler's method, and then corrected iteratively by the modified Euler's method.
3. At $t = 2\Delta t$ the solution is predicted by the two-step Adams-Bashfort method, and then corrected iteratively by the two-steps Adams-Moulton method.
4. At $t = 3\Delta t$ the solution is predicted by the three-step Adams-Bashfort method, and then corrected iteratively by the three-step Adams-Moulton method.
5. At $t = n\Delta t$, $n \geq 4$ for the solution is predicted and corrected by the fourth order modified Hamming's method [9].

It is important to remark that, Lagrange's multipliers are obtained at every time step as part of the solution.

Due to the constraints, this kind of systems usually shows some instabilities which can be easily suppressed by using the Baumgarte's stabilization scheme [15].

This integration methodology allows solving problems in which acceleration terms are present on both sides of the governing equations. This is a requirement since the aerodynamic loads depend on acceleration, velocity, position and orientation of the blades, and the estimation of these forces must be carried out at integer multiples of the time steps. In general the aerodynamic loads computation represents the highest computing cost, and its evaluation inside the time steps would be very expensive.

5. Results

In this section, we present the results obtained with the computational tool based on the developed model. Simulations were carried out for a standard three-bladed LHAWT with 45 m blades and a 68 m tower, which is virtually erected in a flat terrain with very low building density as any rural zone. The structural model has a total of thirteen DoFs, which includes three for the tower, one for the rotor and three for each blade.

In the present effort, the cases of study focus on the response of the LHAWT under different wind conditions while keeping the yaw and pitch configurations fixed. To reach this goal we consider two different wind speeds, 15 and 20 m/s, at which the responses of the tower, rotor and blades are investigated. It is important to remark that these are reference values for the land-surface boundary layer, since the wind profile is not constant since the velocity of the wind varies with height.

5.1. *Case:* $v_{wind} = 15$ *m/s*

In Fig. 1, the rotor angular speed is plotted as a function of revolutions. The rotor speed increases gradually until it reaches the steady state after one and half revolutions. This is due to the power rate of the generator and the aerodynamic damping. In the steady state, the angular speed is approximately 7.2 RPM and the mean produced power is 1.14 MW.

In Fig. 2, the after-forward displacement of the tower top is plotted. The tower bends forward and vibrates with small amplitude around an equilibrium position. This behavior is dominated by the gravitational loads due to the heavy masses, hub, nacelle and blades, located in the front part of the tower. These actions predominate over the aerodynamic loads which push the tower backwards.

In Fig. 3, the side-to-side displacement at the tower top is plotted. The tower bends to the left because the generator produces a reacting moment when it takes energy from the rotor (power rate) which rotates clock-wise. The tower vibrates around an equilibrium position, but the amplitude is higher than that of the after-forward displacement.

In Fig. 4, the flap-wise displacements of the blade tips are plotted. The blades bend up and vibrate; the mean value depends on the aerodynamic loads but the amplitude of the

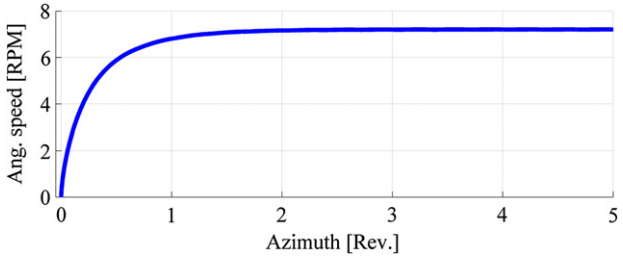

Fig. 1 – Rotor angular speed.

Please cite this article in press as: Gebhardt CG, et al., Non-linear aeroelastic behavior of large horizontal-axis wind turbines: A multibody system approach, International Journal of Hydrogen Energy (2012), doi:10.1016/j.ijhydene.2011.12.090

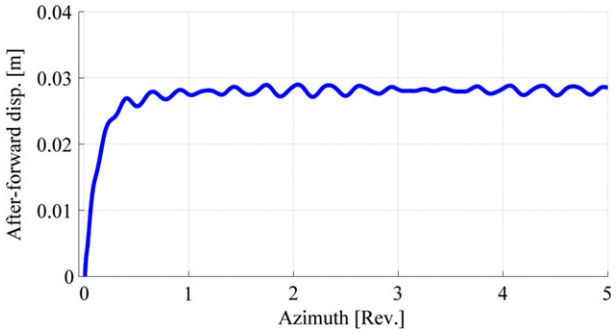

Fig. 2 – After-forward displacement of the tower.

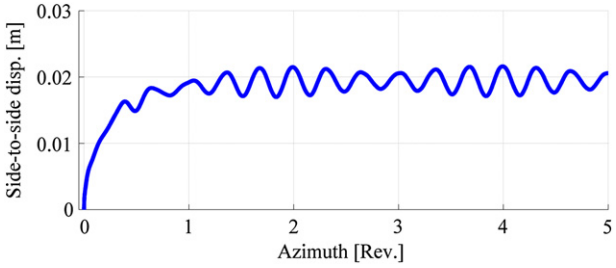

Fig. 3 – Side-to-side displacement of the tower.

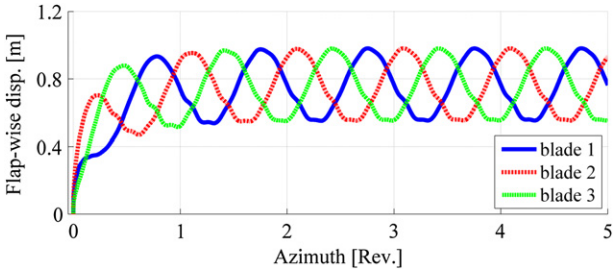

Fig. 4 – Flap-wise displacement of the blades.

vibration is primary governed by gravitational loads. It is very important to remark that the responses of the blades present a phase shift of a one third of a revolution among them; this fact shows coherence respect to the geometric configuration of the rotor.

In Fig. 5, the edge-wise displacements of the blades tips are plotted. The blades vibrate in the edge direction with a mean

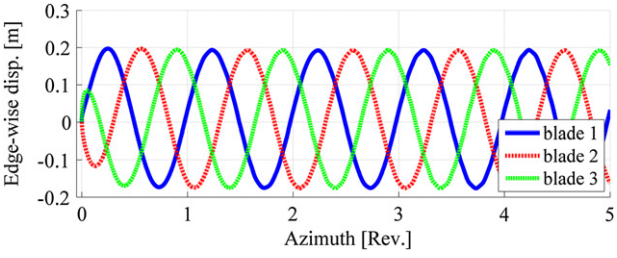

Fig. 5 – Edge-wise displacement of the blades.

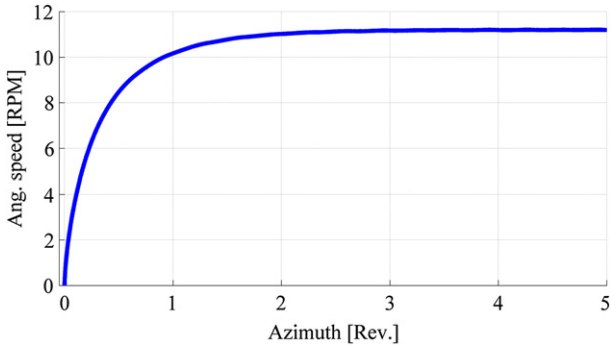

Fig. 6 – Rotor angular velocity.

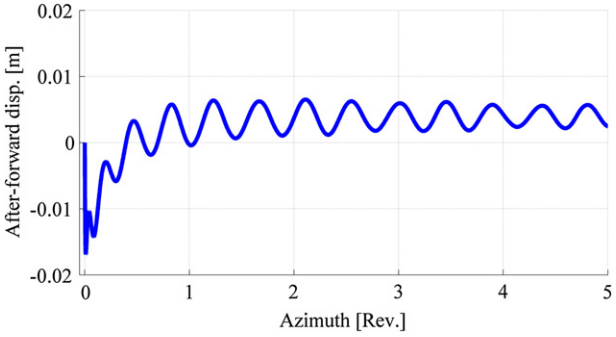

Fig. 7 – After-forward displacement of the tower.

value close to the undeformed position, because the gravitational forces prevail, so when the blades are climbing or falling, they encounter almost the same load distribution but with opposite sign.

5.2. *Case:* $v_{wind} = 20$ *m/s*

In Fig. 6, the rotor angular speed is plotted. The rotor speed shows the same trend of the previous case but in the steady state, the angular speed is approximately 11.2 RPM and the mean produced power is 2.75 MW. Despite the 33% increase in wind speed, the angular speed and mean produced power increase 55% and 141%, respectively. This fact shows the non-linear characteristic of the current problem.

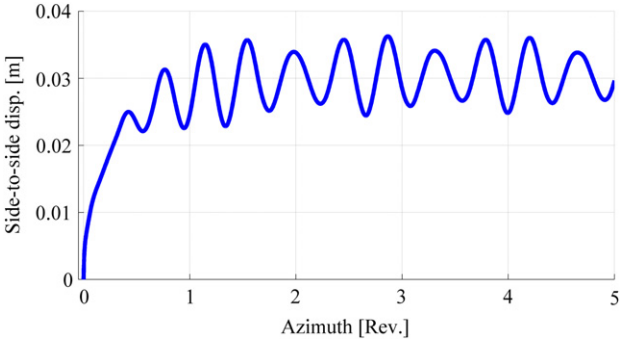

Fig. 8 – Side-to-side displacement of the tower.

Please cite this article in press as: Gebhardt CG, et al., Non-linear aeroelastic behavior of large horizontal-axis wind turbines: A multibody system approach, International Journal of Hydrogen Energy (2012), doi:10.1016/j.ijhydene.2011.12.090

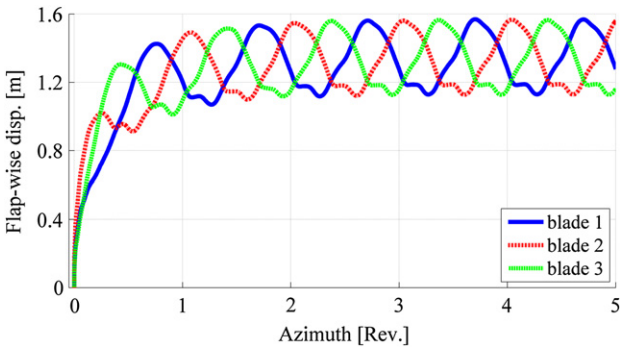

Fig. 9 – Flap-wise displacement of the blades.

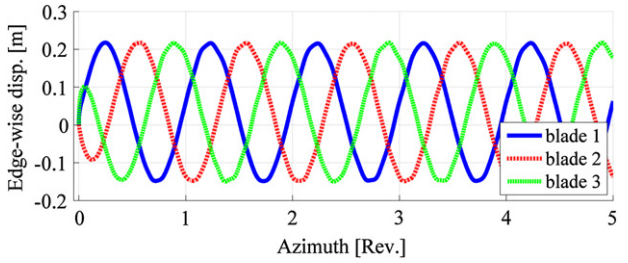

Fig. 10 – Edge-wise displacement of the blades.

In Fig. 7, the after-forward displacement of the tower top is plotted. The tower bends backwards and returns close to the undeformed position with a positive mean value. From this point, the tower vibrates with small amplitude because the aerodynamic loads do not longer prevail; after some time, only gravitational loads remain important even aerodynamic damping, which is essentially proportional to the squared wind velocity, can still be observed. Note that this behavior is different from the one observed in Fig. 2.

In Fig. 8, the side-to-side displacement of the tower top is plotted. As in the previous case, the tower bends to the left and vibrates but this time the mean value increase 63%.

In Fig. 9, the flap-wise displacements of the blade tips are plotted. As in the previous case, the blades bend up showing the same trend, but the mean value increases 79% and the amplitude does changes significantly.

In Fig. 10, the edge-wise displacements of the blades tips are plotted. As in the previous case, the blades vibrate. Although the mean value and the amplitude increase a little, changes are no relevant since gravitational forces predominate.

6. Concluding remarks

It can be concluded that, as the wind speed increases, the steady state angular speed and the produced power also increase. However, the second grows faster and shows a strong non-linear behavior.

The after-forward displacement of the tower strongly depends on the gravitational loads when the wind speed is not very large, but as the wind speed increases the aerodynamic loads become more and more relevant.

The side-to-side displacement of the tower depends on the aerodynamic loads and the power rate of the electrical generator.

The mean value of the flap-wise displacement mainly depends on the aerodynamic loads. However, the amplitude of the vibrations mainly is governed by the gravitational loads.

The edge-wise displacement mainly depends on the gravitational loads and it does not change significantly when the wind speed varies.

Although the proposed model constitutes a good starting point to get an understanding of the aeroelastic behavior of LHAWTs, in the future, it will be necessary to expand the present ideas and add a very precise model of the power generation dynamics, the dynamics of the electrical network and/or the dynamics associated to a hydrogen production system based on wind energy.

REFERENCES

[1] Petersen JT. Kinematicly non-linear finite element model of a horizontal-axis wind turbine. Ph.D. Thesis: Risø National Laboratory; 1990.
[2] Lee DL, Hodges DH, Patil MJ. Multi-flexible-body dynamic analysis of horizontal-axis wind turbines. Wind Energy 2002; 5:281–300.
[3] Jonkman JM, Buhl Jr ML. FAST user's guide. Technical report NREL/EL-500-8230. NREL; 2005.
[4] Zhao X, Maiβer P, Wu J. A new multi-body modeling methodology for wind turbine structures using a cardanic joint beam element. Renew Energ 2007;32:532–46.
[5] Kallesøe BS. Equations of motion for a rotor blade, including gravity, pitch action and rotor speed variations. Wind Energy 2007;10:209–30.
[6] Hodges DH, Dowell EH. Nonlinear equations of motion for the elastic bending and torsion of twisted nonuniform rotor blades. Technical report TN D-7818. NASA; 1974.
[7] Maiβer P. Analytical dynamics of multi-body systems. Comput Method Appl M 1991;91:1391–6.
[8] Heard WB. Rigid body mechanics: mathematics, physics and applications. Wiley; 2006.
[9] Preidikman S. Numerical simulation of interactions among aerodynamics, structural dynamics, and control systems. Ph.D. Thesis: Virginia Polytechnic Institute; 1998.
[10] Meirovith L. Computational methods in structural dynamics. Springer; 1980.
[11] Kane TR, Ryan RR, Banerjee AK. Dynamics of a cantilever beam attached to a moving base. J Guid Control 1987;10: 139–51.
[12] Nikravesh PE. Computer-aided analysis of mechanical systems. Prentice-Hall; 1988.
[13] Shabana AA. Dynamics of multibody systems. Cambridge University Press; 2010.
[14] Gebhardt CG, Preidikman S, Massa JC. Numerical simulations of the aerodynamic behavior of large horizontal-axis wind turbines. Int J Hydrogen Energy 2010;35:6005–11. doi:10.1016/j.ijhydene.2009.12.089.
[15] Baumgarte J. Stabilization of constrains and integrals of motion in dynamic systems. Comput Method Appl M 1972;1: 1–16.

Please cite this article in press as: Gebhardt CG, et al., Non-linear aeroelastic behavior of large horizontal-axis wind turbines: A multibody system approach, International Journal of Hydrogen Energy (2012), doi:10.1016/j.ijhydene.2011.12.090